

We are IntechOpen, the world's leading publisher of Open Access books Built by scientists, for scientists

6,900

Open access books available

186,000

International authors and editors

200M

Downloads

Our authors are among the

154

Countries delivered to

TOP 1%

most cited scientists

12.2%

Contributors from top 500 universities



WEB OF SCIENCE™

Selection of our books indexed in the Book Citation Index
in Web of Science™ Core Collection (BKCI)

Interested in publishing with us?
Contact book.department@intechopen.com

Numbers displayed above are based on latest data collected.
For more information visit www.intechopen.com



Crystal Structure and Solid-State Properties of Metal Complexes of the Schiff Base Ligands Derived from Diacetylmonoxime: A Brief Review

*Palash Mandal, Uttam Das, Kamalendu Dey
and Saikat Sarkar*

Abstract

The fabulous advancement of a large section of modern coordination chemistry depends upon different kinds of strategically designed and functionally tuned ligand systems; Schiff base ligands play a pivotal role among them. Such Schiff bases become more motivating when they are designed to be synthesized using very simple organic molecules. This paper reviews our work on a family of three functionally different types of Schiff base ligands, derived from diacetylmonoxime, which have been employed to synthesize mononuclear metal complexes with various binding modes of ligands and topologies around the metal centers. Such Schiff base ligands have been synthesized by reacting diacetylmonoxime with diethylenetriamine, 1,3-diaminopropane-2-ol, and morpholine N-thiohydrazide. The synthesized Schiff bases and the metal complexes of such “privileged ligands” show many interesting supramolecular coordination architectures involving different weak forces, e.g., H-bonding, C–H \cdots π interactions, etc.

Keywords: Schiff base, diacetylmonoxime, crystal structure, weak force interactions, semiconducting behavior, optical properties

1. Introduction

The synthesis and characterization of metal complexes of Schiff bases have been started since 1865. But the importance of Schiff base ligands in several fields compelled us to consider it as a “privileged ligand” even in recent days [1, 2]. Currently, there has been considerable interest in the chemistry of Schiff base metal complexes, primarily because of their tremendous biochemical activity, viz., antibacterial [3, 4], antimalarial [5, 6], antiviral [7, 8], and antitumor activities [9–11]. Besides, some transition metal Schiff base complexes were found to be efficient catalysts in organic synthesis [12–18]. Such types of Schiff base metal complexes are also very interesting for opening of a new pathway in crystal engineering [19, 20]. Various kinds of supramolecules of diverse fascinating structures are being

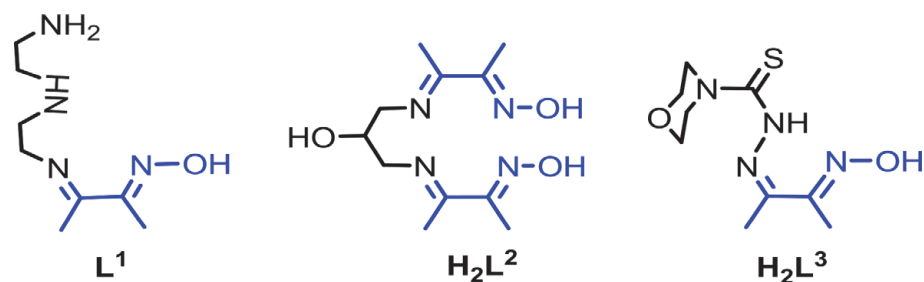


Figure 1.
Structural drawing of the ligand systems.

synthesized by different Schiff bases [20, 21]. Different types of weak force interactions (e.g., H-bonding, $\pi \cdots \pi$, C–H $\cdots\pi$, etc.) are responsible for construction of such new metal organic frameworks (MOF) [22–24]. Multinuclear metal complexes of Schiff base are of real importance on the field of magnetochemistry [25–28]. Various ferro- and antiferro-type magnetic interactions are responsible for the generation of different magnetic materials. Besides, the solid-state properties, e.g., variable temperature conductivity, and optical properties of such complexes are also producing very interesting results which are extremely important in materials chemistry. Very recently the comparison of different observed physical properties with the theoretically predicted values is being done by the use of DFT approach [29–32].

In the above context, the development of new pathways for the synthesis of new Schiff base ligands and their metal complexes is of immense significance. The strategic pathway becomes more important when the Schiff base ligands and their corresponding metal complexes are produced in a controlled approach fulfilling the main objectives of the synthesis. We have chosen easily available, exceptionally economical, and full of exciting properties organic molecule, diacetylmonoxime, as our precursor molecule for the synthesis of many new Schiff base ligands by reacting it with different molecular amine systems. One of the main advantages of such Schiff base ligands is the change in their ligational behavior depending on the metallic systems and the stoichiometry.

In this review, we have selected only three Schiff base ligands (**Figure 1**) derived from diacetylmonoxime and three different amine systems. Though a huge number of metal complexes have been synthesized and characterized using such ligand systems, only the structure of the ligands and metal complexes for which single crystal or PXRD have been determined, are discussed in this mini-review including the weak force interactions depicted therein. Some of the solid-state properties, viz., electrical and optical properties of such complexes, are also discussed to enlighten their fascinating material properties.

2. Synthesis of the ligands

2.1 Mono-imine Schiff base (L^1) ligand

The stoichiometrically controlled condensation reaction of diacetylmonoxime (dam) (1.01 g, 10 mmol) and diethylenetriamine (dien) (1.04 g, 10 mmol) in 1:1 molar ratio in methanol (15 ml) on constant stirring for 45 min at room temperature and then refluxing for 2 h on water bath (**Figure 2**) afforded the monocondensed amine-imine-oxime Schiff base ligand 3-((2-((2-aminoethyl)-amino)ethyl)imino)butan-2-one oxime (L^1). Yield is 55% [29].

2.2 Di-imine Schiff base (H_2L^2) ligand

The condensation reaction of 1,3-diaminopropane-2-ol (0.45 g, 5 mmol) (dapol) with diacetylmonoxime (1.01 g, 10 mmol) in 1:2 molar ratio in methanol (25 ml) under gentle reflux for 2 h yielded the tetradentate bicondensed di-imine Schiff base 3,3'-((2-hydroxypropane-1,3-diyl)bis(azanylylidene))bis(butan-2-one) dioxime (H_2L^2) (**Figure 3**). Yield is 65% [33].

2.3 Thio-hydrazone Schiff base (H_2L^3) ligand

The condensation reaction of diacetylmonoxime (1.01 g, 10 mmol) with morpholine N-thiohydrazide (mth) (1.6 g, 10 mmol) in 1:1 molar ratio in ethanol (30 ml) on refluxing for 2 h afforded a gummy mass with very low yield. The isolation of solid ligand in pure form with high yield is still a challenge. Considering the low yield of the ligand, all the complexation reactions with this ligand were carried out under in situ condition. However, the molecular thiol form of the ligand H_2L^3 (**Figure 4**) was established from the structural analysis (single-crystal X-ray diffraction) of its metal complexes [34–36].

A slight modification of synthetic procedure by continuing the refluxing procedure for 16 h with few drops of water in 1:1 molar ratio in ethanol (50 ml) (shown in the left part of **Figure 4**) yielded a light yellow crystalline solid compound (yield 45%). X-ray diffraction study of single crystal along with other analytical data of this compound inferred a zwitterionic structure of a nitrogen–sulfur heterocyclic compound, N-(3,4-dimethyl-1,2,5-thiadiazole-2-ium-2-yl)morphine-4-carbathio-ate (abbreviated as L^4) [25]. Metal complexes with L^4 have not been reported yet.

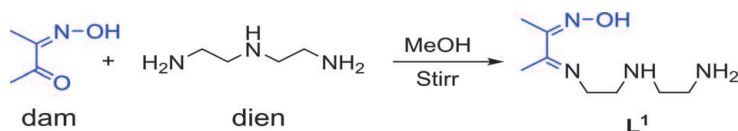


Figure 2.
Scheme of formation of ligand L^1 .

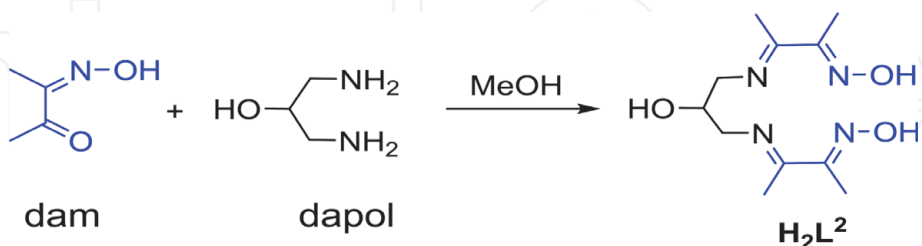


Figure 3.
Scheme of formation of ligand H_2L^2 .

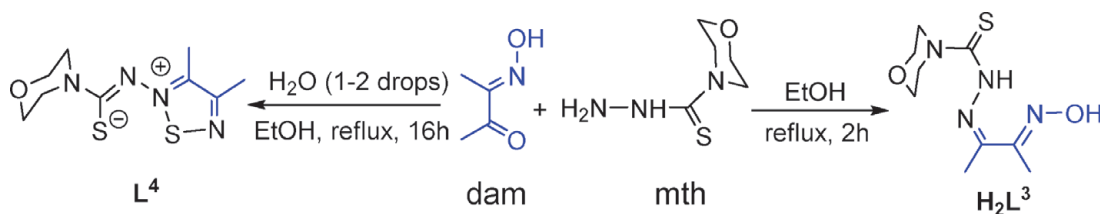


Figure 4.
Scheme of formation of ligand H_2L^3 and zwitterionic heterocycle (L^4).

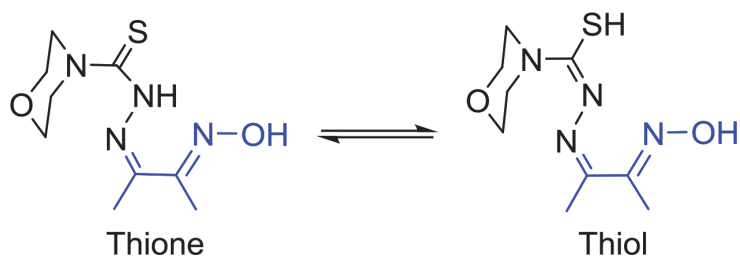


Figure 5.
Thione-thiol tautomerism.

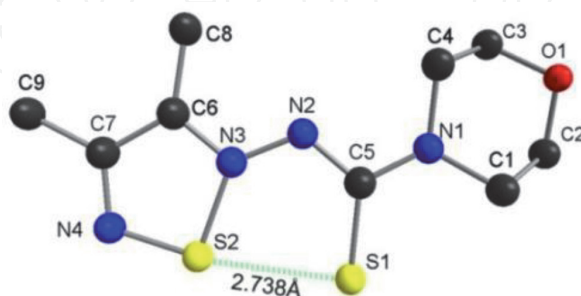


Figure 6.
Perspective view of the ligand L^4 with atom number scheme (hydrogen atoms are omitted for clarity).

The hydrogen atom attached with N atom of hydrazide group can undergo thione-thiol tautomerism (**Figure 5**). Thus NNS coordination mode is facilitated during the formation of complexes [34].

2.3.1 Crystal structure of L^4

The molecular structure of L^4 was established with the single-crystal X-ray diffraction studies. It was observed that the N–N, N–C, and C–S bond distances are shorter than the corresponding single bond distances indicating a partial double bond character due to resonance stabilization using π -bonded electrons. The morpholine moiety preferred chair conformation in the solid state. The distance between the nonbonded $S \cdots S^-$ is 2.738 Å, and weak interactions (**Figure 6**) were observed between them in the solid state. A two dimensional supramolecular network is formed by the H-bonding and π - π interactions [34].

3. Synthesis of metal complexes

3.1 Metal complexes with mono-imine Schiff base (L^1) ligand

With this new neutral N_4 donor ligand system, a crystalline Ni(II) complex has been synthesized. Two routes of synthesis of the nickel complex (**complex 1**) were reported (**Figure 7**). According to **Route 1**, the nickel complex was synthesized by in situ reaction of an equimolar mixture of diacetylmonoxime (1.01 g, 10 mmol) and diethylenetriamine (1.04 g, 10 mmol) and $Ni(SCN)_2 \cdot 4H_2O$ (2.47 g, 10 mmol) in methanol under reflux condition, which produces $[Ni(L^1)(SCN)_2]$ (**complex 1**). In **Route 2**, **complex 1** was synthesized by following the same steps, but nickel chloride ($NiCl_2 \cdot 6H_2O$) (2.37 g, 10 mmol) was used instead of $Ni(SCN)_2$ and then by treating the product with NH_4SCN (1.52 g, 20 mmol) in aqueous-methanol (1:1, 10 ml). Pure crystals (single) were obtained from the slow evaporation of the

mother liquor. Yields of the **complex 1** in the routes 1 and 2 are 85% and 82% respectively [29].

3.2 Metal complex with di-imine Schiff base (H_2L^2) ligand

The di-imine Schiff base ligand (H_2L^2) was employed for the synthesis of a oxovanadium complex, the PXRD of which have also been determined. Reflux of equimolecular mixture of H_2L^2 (1.28 g, 5 mmol) and vanadyl acetate (0.93 g, 5 mmol) in methanol (30 ml) (**Figure 8**) afforded the greenish-gray complex of vanadium (**complex 2**), having composition $[VO(L^2)]$. In this complex the ligand is found to act as a dibasic N_4 donor system [33].

3.3 Metal complexes with thio-hydrazone Schiff base (H_2L^3) ligand

The thio-hydrazone Schiff base ligand (H_2L^3) is very interesting, and the thiol form of the Schiff base is always observed for the binding purposes (see **Figure 5**) with the metal systems during complexation. Most interestingly, this ligand is found to show two types of binding modes (**Figure 9**), one is observed through N,S donor atoms and another one through N,N,S donor atoms. An efficient control over the ligand for binding through either N,S or N,N,S mode has been achieved though specific choice of metal systems [34–38].

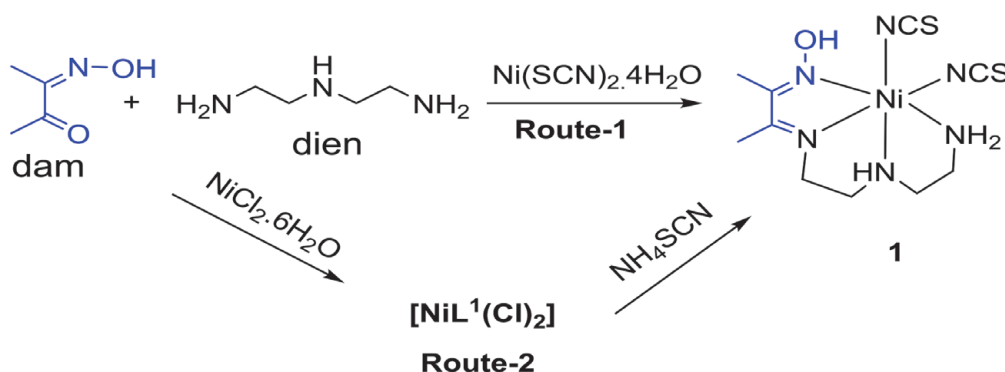


Figure 7.
Scheme of preparation of Ni(II) complexes.

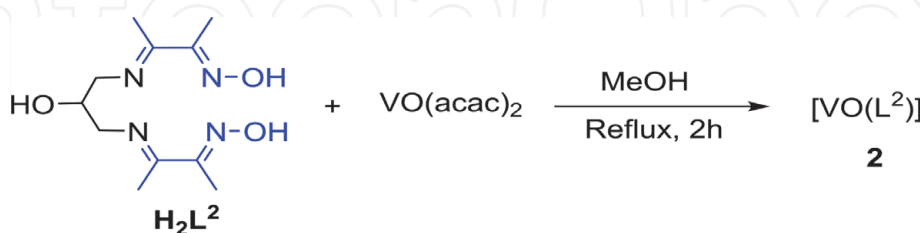


Figure 8.
Scheme of preparation of VO(IV) complex.

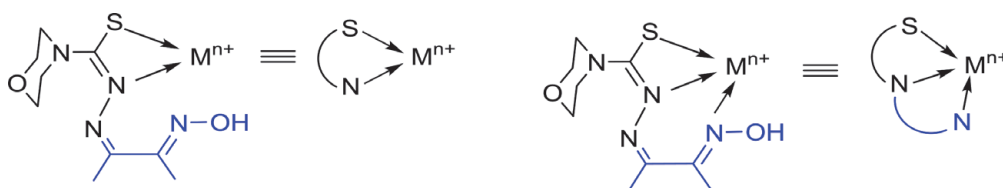


Figure 9.
Different modes of binding of H_2L^3 ligand.

An organometallic complex, $[\text{PhHg}(\text{HL}^3)]$ (**complex 3**), and the zinc(II) complex $[\text{Zn}(\text{HL}^3)(\text{OAc})(\text{H}_2\text{O})]$ (**complex 4**) were prepared by the gentle reflux of the equimolar quantities of diacetylmonoxime (0.5 g, 5 mmol) and morpholine N-thiohydrazide (0.8 g, 5 mmol) (**Figure 10**) in the presence of the respective metal salts, $[\text{PhHg}(\text{OAc})]$ (1.68 g, 5 mmol) and $[\text{Zn}(\text{OAc})_2] \cdot 2\text{H}_2\text{O}$ (1.1 g, 5 mmol). Yields of the complexes are 65% (**3**) and 75% (**4**). The pure single crystals of the complexes were obtained from their chloroform solutions [34, 35].

The Cd(II), Cr(III), and Fe(III) complexes, i.e., $[\text{Cd}(\text{HL}^3)_2]$ (**complex 5**), $[\text{Cr}(\text{HL}^3)_2]\text{Cl} \cdot 3\text{H}_2\text{O}$ (**complex 6**), and $[\text{Fe}(\text{HL}^3)_2]\text{Cl} \cdot 3\text{H}_2\text{O}$ (**complex 7**), were prepared by the gentle reflux of the mixture of diacetylmonoxime (0.5 g, 5 mmol) and morpholine N-thiohydrazide (0.8 g, 5 mmol) and the respective metal salts ($[\text{Cd}(\text{OAc})_2] \cdot 2\text{H}_2\text{O}$ (0.67 g, 2.5 mmol), $\text{CrCl}_3 \cdot 6\text{H}_2\text{O}$ (0.67 g, 2.5 mmol), and $\text{FeCl}_3 \cdot 6\text{H}_2\text{O}$ (0.68 g, 2.5 mmol) in the ratio of 2:2:1 (**Figure 10**). Yields of the complexes had been recorded as 75% for each complex. The pure single crystals of the complexes were obtained from their chloroform solutions [35, 36].

Another zinc(II) complex (**complex 8**) was synthesized by the reflux of the mixture of diacetylmonoxime (0.5 g, 5 mmol) and morpholine N-thiohydrazide (0.8 g, 5 mmol) in the presence of $\text{Zn}(\text{OAc})_2 \cdot 2\text{H}_2\text{O}$ (0.55 g, 2.5 mmol) in the molar ratio of 2:2:1 in water–methanol (1:1, v/v) mixture (**Figure 11**). The yellow colored complex of composition $[\text{Zn}(\text{HL}_3)_2] \cdot 2\text{H}_2\text{O}$ had been separated with 60% yield and recrystallized from chloroform [37].

The complexes of Ni(II) (**complex 9**), Co(II) (**complex 10**), and Cu(II) (**complex 11**) were synthesized by gentle reflux of three sets of equimolar quantities of diacetylmonoxime (0.5 g, 5 mmol) and morpholine N-thiohydrazide (0.8 g, 5 mmol) in the presence of the metal salts $[\text{Ni}(\text{OAc})_2] \cdot 4\text{H}_2\text{O}$ (1.24 g, 5 mmol), $[\text{Co}(\text{OAc})_2] \cdot 4\text{H}_2\text{O}$ (1.25 g, 5 mmol), and $[\text{Cu}(\text{OAc})_2] \cdot 4\text{H}_2\text{O}$ (1.28 g, 5 mmol), respectively) in ethanol (50 ml) (**Figure 11**) [29]. General molecular formula of the metal complexes **9–11** is $[\text{M}^{\text{II}}(\text{HL}^3)(\text{OAc})]$ where M stands for Ni, Co, and Cu.

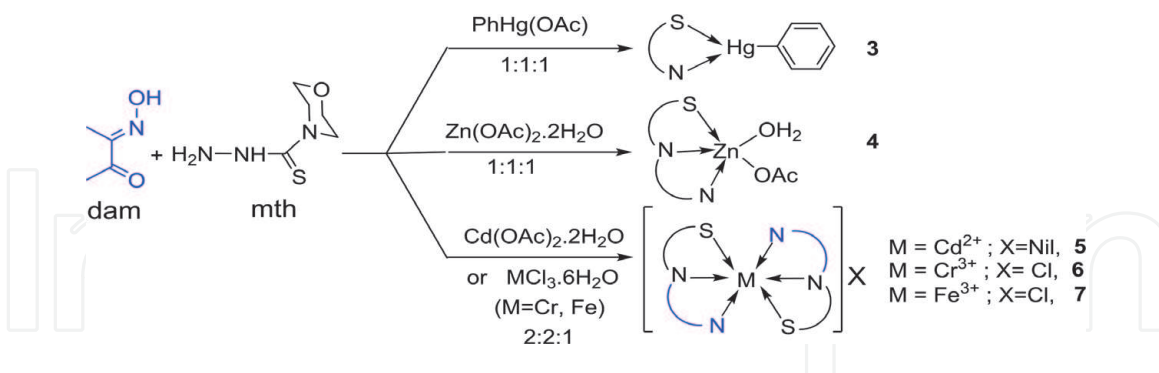


Figure 10.

Scheme of formation of metal complexes using H_2L^3 ligand indicating different binding pattern.

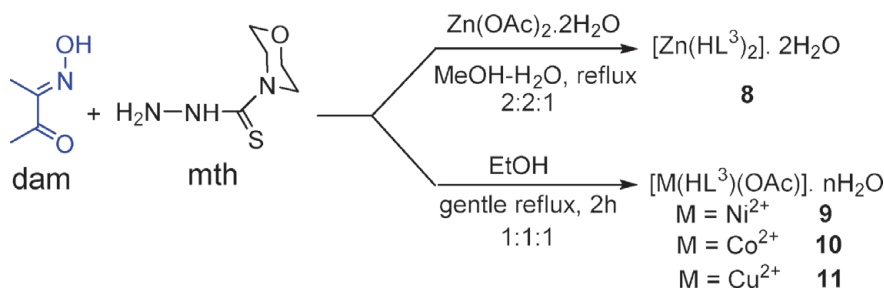


Figure 11.

Scheme of preparation of other metal complexes using H_2L^3 ligand.

4. Crystal structures, PXRD, and some interesting properties of the metal complexes

4.1 Crystal structure and catalytic properties of nickel(II) complex with the mono-imine Schiff base ligand (L^1)

The neutral monomeric complex $[Ni(L^1)(NCS)_2]$ (**1**) has been found to possess octahedral geometry where central Ni(II) is coordinated by the neutral ligand L^1 with tetradentate N_4 binding mode and two N-bonded thiocyanate ions occupying the *cis*-position. **Figure 12** depicts the molecular structure of the nickel (II) complex **1** [29].

The coordination environment around the nickel(II) ion is surrounded by N_6 fashion (four N from ligand and two N from thiocyanate ions) tending towards distorted octahedral geometry. The Ni^{2+} center is not lying exactly within the equatorial plane of N_4 moiety, and unequal axial and equatorial bond distances (2.112 Å and 2.072 Å, respectively) confirm the distortion. The non-coordinated O–H groups on the ligand L^1 are engaged in H-bonding interactions with thiocyanate S atoms (**Figure 6**) which lead to 1D supramolecular sheet-like arrangement (**Figure 13**). These H-bonding interactions lead to O...S separations of 3.132 Å and play prominent role in crystal packing.

4.1.1 Catalytic activity of complex **1**

Analytical grade reagents and freshly distilled solvents, viz., water, acetonitrile, methanol, and dichloromethane, were used to check the catalytic activity. The oxidation reaction was carried out in liquid phase under vigorous stirring in two-necked round bottom flask fitted with a water condenser and placed in an oil bath at 60°C. Substrate (5 mmol) was taken in 10 ml solvent(s) for different sets of reactions along with 5 mg catalyst, to which 10 mmol of *tert*-Butyl hydrogen peroxide

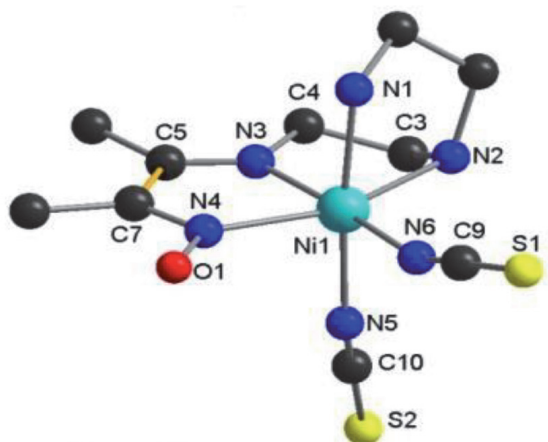


Figure 12.
Perspective view of complex **1** with atom numbering scheme (hydrogen atoms are omitted for clarity).

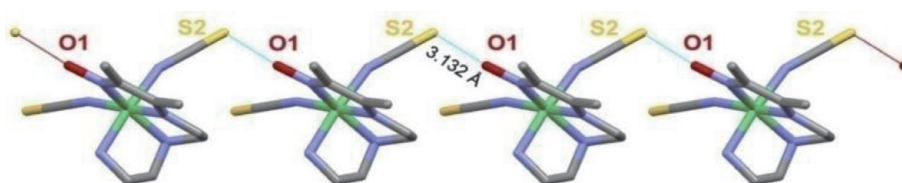


Figure 13.
 $S \cdots O$ interaction in the crystal of complex **1** (hydrogen atoms are omitted for clarity).

(TBHP, 70% aq.) was added as oxidant immediately before the start of the reaction. Aliquots of the reaction mixture were withdrawn at various time intervals, and the products were analyzed by using Agilent 6890A gas chromatograph equipped with HP-1 capillary column and FID. All reaction products were identified and estimated by using an Agilent GC-MS (QP-5050 model).

The $[\text{Ni}(\text{L}^1)(\text{NCS})_2]$ (**1**) exhibits good catalytic activity towards the oxidation of styrene in the presence of TBHP which leads to the formation of benzaldehyde as a major product with small amount of styrene oxide as shown in **Figure 14**. By varying solvents, reaction time, temperature, and substrate-to-oxidant ratio, a successful conversion of 70% of the styrene was reached at the optimum condition [29].

4.2 PXRD structure and solid-state properties of oxovanadium(IV) complex with the di-imine Schiff base ligand (H_2L^2)

Despite our repeated attempts and best effort, the single crystal of the oxovanadium(IV) complex with the ligand H_2L^2 could not be grown, and it led us to carry out the powder X-ray diffraction (PXRD) study to characterize the oxovanadium(IV) complex **2**. The composition of the complex is $[\text{VO}(\text{L}^2)]$, where the ligand H_2L^2 acts as a dibasic $[(\text{L}^2)^{2-}]$ tetradentate arrangement. The result of the PXRD shows that the unit cell is monoclinic in nature and the cell parameters of the complex **2** are $a = 16.0619 \text{ \AA}$, $b = 11.5517 \text{ \AA}$, $c = 12.7262 \text{ \AA}$, and $\beta = 122.427^\circ$; and the cell volume (V) is 1993.05 \AA^3 .

Other solid-state properties, viz., electrical, optical, and thermal properties of the complex $[\text{VO}(\text{L}^2)]$, have also been studied [24]. The complex is electrically an insulator at room temperature; however, the conductivity is increased as the temperature increases from 330 K, indicating the semiconducting nature of the complex. It behaves as an n-type semiconductor, and the semiconducting behavior of the oxovanadium(IV) complex with the dibasic Schiff base ligand was substantiated by the extended conjugated chemical structure. The said properties are discussed in detail in the following sections.

4.3 Crystal structures and properties of metal complexes with thio-hydrazone Schiff base ligand (H_2L^3)

4.3.1 Crystal structure of organometallic phenylmercury(II) complex (**3**)

The organometallic phenylmercury(II) compound **3** crystallized in triclinic form to give a tricoordinated T-shaped geometry (**Figure 15**). Here the monobasic ligand $[(\text{HL}^3)^-]$ coordinated the central mercury in a bidentate manner through S and N (N of hydrazone function) and the third coordination of the mercury was satisfied by the C atom of phenyl group of the metal precursor. Thus, by choosing the phenylmercury system, the ligand H_2L^3 has been compelled to act in a bidentate mode leaving another N donor (the oxime N) uncoordinated [35].



Figure 14.
Oxidation of styrene using $[\text{Ni}(\text{L}^1)(\text{NCS})_2]$ as catalyst.

The Hg(II) atom remains 0.027(1) Å above the plane. Due to the contribution of electron flow from mercury to the π^* orbitals of the phenyl group, the Hg–C bond distance is found shorter than that in the analogous methylmercury(II) compound, where no such electron drifting is observed. The C–S bond gets partial double bond character in the complex, similar to related thiosemicarbazones of methylmercury (II) and dimethylthallium(III). It is interesting to note that there is no intermolecular π – π interaction between the phenyl rings. But a weak interaction between C(8)–H(8A) and a π group (phenyl ring) links the two phenylmercury molecules into a supramolecular dimer having a C–H π synthon (**Figure 16**) having characteristic H...C_g distance 2.84 Å, where C_g is the midpoint of the phenyl ring.

4.3.2 Crystal structure of the zinc(II) complex (4)

The X-ray crystal structure shows that due to constrained ligand structure, the [Zn(HL³)(OAc)(H₂O)].H₂O complex **4** (**Figure 17**) has adopted distorted square pyramidal geometry ($\tau = 0.05$) in which the oxime nitrogen, azomethine nitrogen, deprotonated thiol sulfur of ligand [(HL³)[−]], and acetato oxygen defines the equatorial plane, while the axial position is occupied by oxygen (O₄) of coordinated

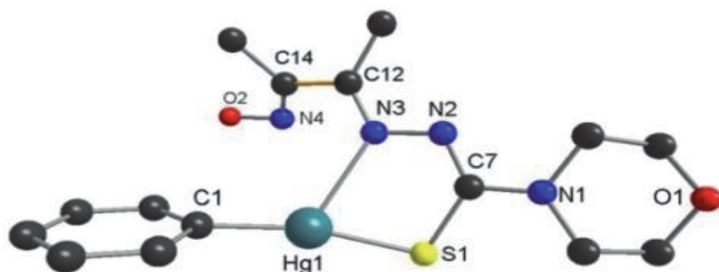


Figure 15.
Perspective view of complex **3** with atom numbering scheme (hydrogen atoms are omitted for clarity).

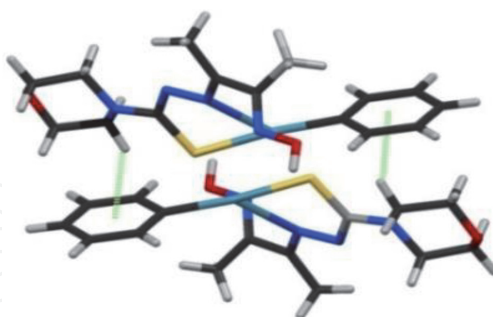


Figure 16.
Weak interaction (C–H... π) between the π -electrons of the phenyl ring with the H atom of ligand in a supramolecular dimer.

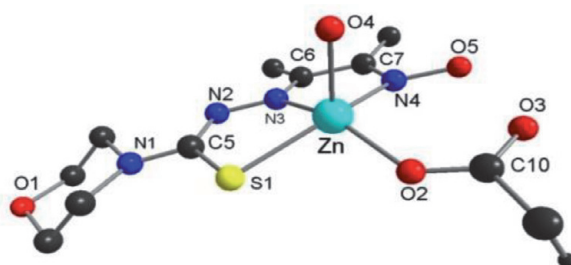


Figure 17.
Perspective view of complex **4** with atom numbering scheme (hydrogen atoms are omitted for clarity).

water molecule. The zinc(II) ion is 0.3766 (8) Å out of the basal plane towards the oxygen (O₄) of coordinated water molecule. The deprotonation of the ligand results in extensive delocalization of charge, and as a consequence the C–S bond length (1.7459(18) Å) is much closer in length to a C–S single bond (1.82 Å), which has partial double bond character [34].

Due to intramolecular hydrogen bonding, the Zn–N(3) (azomethine) distance is slightly shorter than Zn–N(4) (oxime) distance. Here the H(1) of coordinated water molecule is hydrogen bonded to morpholinic oxygen O(1), while H(2) is hydrogen bonded to acetate oxygen O(3), and such H-bonding forms the 1D supramolecular framework diagonal to the *ab* plane (**Figure 18**).

4.3.3 Crystal structure of the cadmium(II) complex (5)

The cadmium(II) complex [Cd(HL³)₂] (5) crystallized in a triclinic space group $P\bar{1}$ (2). The central Cd (II) ion is coordinated by two units of monobasic ligand [(HL³)[−]] forming trapezoidal bipyramid (**Figure 19**), where the equatorial plane was formed by thiol S1, azomethine N3, oxime N4 of one Schiff base unit, and azomethine N7 atoms of another unit (second) and the axial positions are being coordinated by oxime N8 and thiol S2 atoms of the second Schiff base unit. The C–S bond gets partial double bond character in the complex and is shorter than that in phenylmercury(II) complex (3). The C–N average bond distance confirms double bond character, and deprotonation of the hydrazinic NH proton induces double bond character [35].

Complex 5 forms a 2D supramolecular sheet in the *bc* plane through hydrogen bonding interactions (O–H...O and C–H...O) (**Figure 20**). The average D...A separations and the average D–H...A angle is 145°. These supramolecular sheets stack along (100) the plane. There are no directional weak force interactions (π – π , C–H... π , hydrogen bonding) operating between the two sheets. Therefore, an intermolecular van der Waals interaction might be responsible for such supramolecular stacking. The methyl terminals of the ligand from adjacent sheets face each other in this arrangement.

One of the most interesting parts of the structure is that the crystal structure possesses a remarkably short intermolecular C(sp³)...O(sp³) contact [C9...O4* 2.958 (3) Å]. An interesting packing force using an uncommon C(sp³)...O(sp³)

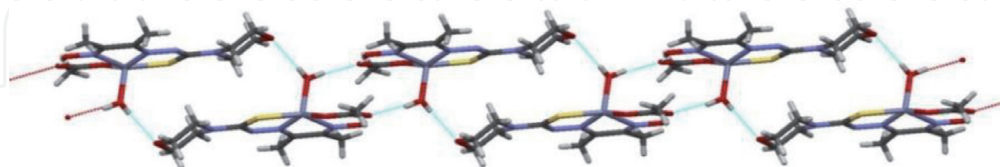


Figure 18.

One-dimensional network through H-bonding in [Zn(HL³)(OAc)(H₂O)]·H₂O.

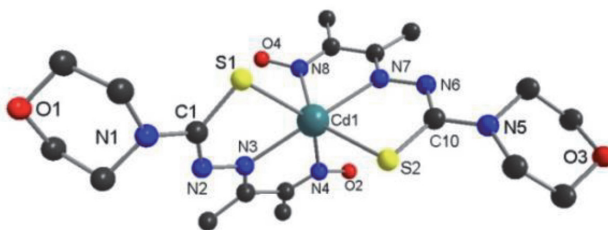


Figure 19.

Perspective view of complex 5 with atom numbering scheme (hydrogen atoms are omitted for clarity).

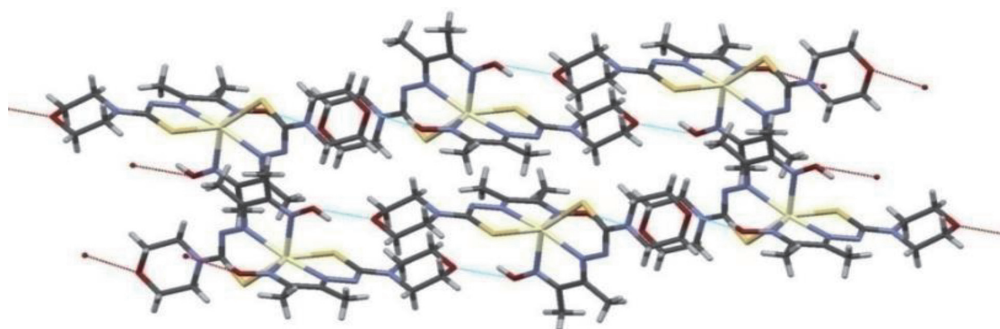


Figure 20.
Two-dimensional network through H-bonding in $[Cd(HL^3)_2]$ (5).

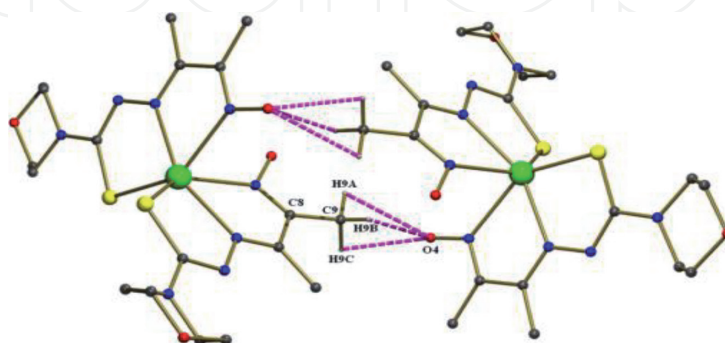


Figure 21.
Trifurcated H-bonding interactions [35] in $[Cd(HL^3)_2]$ (5).

interaction has been reported. The three H atoms (H9A, H9B, H9C) of the methyl group of the propylidene moiety form a triangular plane which is supported by the angle $\angle C8-C9 \cdots O4^*$ of 172.0° . The O4 atom of the oxime is directed towards the center of the plane formed by three H atoms (H9A, H9B, H9C) of the methyl group. The $C9-H9A \cdots O4^*$, $C9-H9B \cdots O4^*$, and $C9-H9C \cdots O4^*$ angles are 89.0° , 83.8° , and 97.6° , respectively, which are less than the generally accepted $\angle C-H \cdots O$ angles (110°), and such short bond angles might be responsible for the greater $C \cdots O$ attraction. Thus, the cooperative effect of the three individual interactions acts on the face of the plane of the three methyl hydrogens of the C9 atom due to their high acidic character. This very unusual and nonconventional interaction was termed as a $CH_3 \cdots O$ interaction and proved to be a good supramolecular synthon. The trifurcated H-bonding interactions are shown in (Figure 21).

4.3.4 Crystal structure of the chromium(III) complex (6)

The X-Ray single-crystal analysis revealed that complex $[Cr(L^3)_2]Cl \cdot 3H_2O$ (6) forms slightly distorted octahedral geometry with $[CrN_4S_2]$ core having meridional conformation via the oximino N, imine N, and thiol S atoms (Figure 22), i.e., the two monobasic tridentate L^3 ligands act as N,N,S donor during formation of the complex [36].

4.3.5 Crystal structure of the iron(III) complex (7)

The X-ray structure of $[Fe(L^3)_2]Cl \cdot 3H_2O$ (7) is quite similar to that of complex (6) with pseudo-octahedral geometry except that the equatorial plane is formed by two oximino N atoms and two thiol S atoms and the axial positions are occupied by two imine N atoms of the ligand (Figure 23). The Fe–N(imine) bond lengths are significantly shorter than the Fe–N(oximino) bond lengths because azomethine

nitrogen is a stronger base than the oximino nitrogen. The deprotonation of the ligands results in extensive delocalization of charge, and thus the C–S bond gets partial double bond character [36].

The most interesting part of the crystalline structure of complex $[\text{Cr}(\text{L}^3)_2]\text{Cl}\cdot 3\text{H}_2\text{O}$ (6) and $[\text{Fe}(\text{L}^3)_2]\text{Cl}\cdot 3\text{H}_2\text{O}$ (7) is that both the complexes form a 1D supramolecular chain along the *c*-axis through C–H \cdots O interactions between each molecule (**Figure 24**).

The 1D chains are arranged in parallel direction to form a supramolecular host having channels along the *c*-axis (**Figure 25**). Such channels are filled by self-assembled “water-chloride” clusters having chair conformation (**Figure 25**).

It is proven by the crystal structure analysis that there are three crystals of water molecules per formula unit of **complexes 6** and **7** along with chloride ion, and these are involved in forming the infinite “water-chloride” cluster [36] with a chair

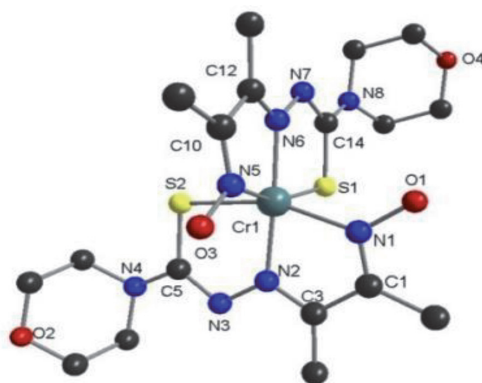


Figure 22.

Perspective view of complex **6** with atom numbering scheme (hydrogen atoms are omitted for clarity).

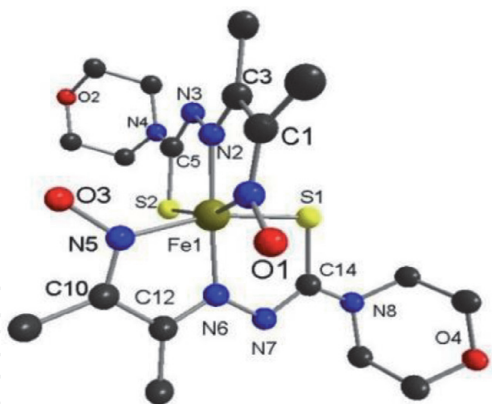


Figure 23.

Perspective view of complex **7** with atom numbering scheme (hydrogen atoms are omitted for clarity).

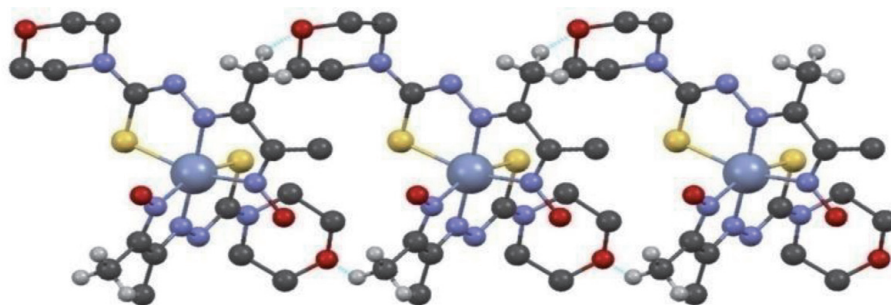


Figure 24.

One-dimensional network through C–H \cdots O interactions in complexes (**6**) and (**7**).

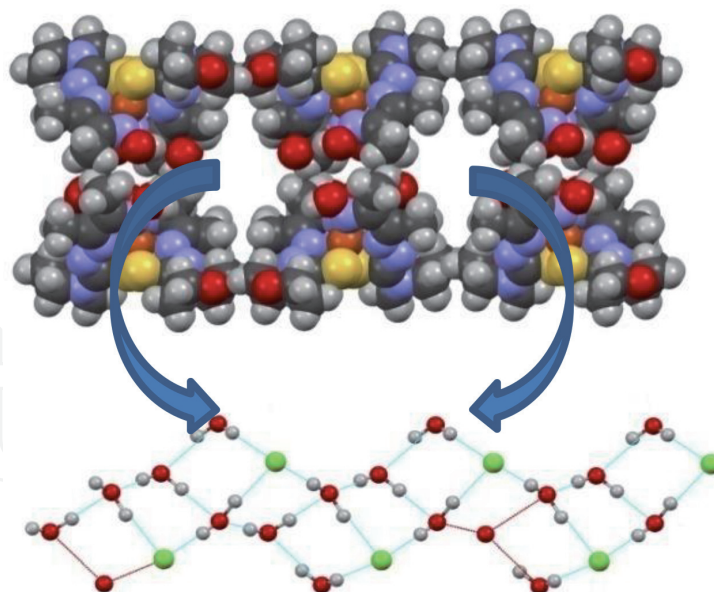


Figure 25.
Supramolecular channels and “water-chloride” cluster along the c-axis in complexes (6) and (7).

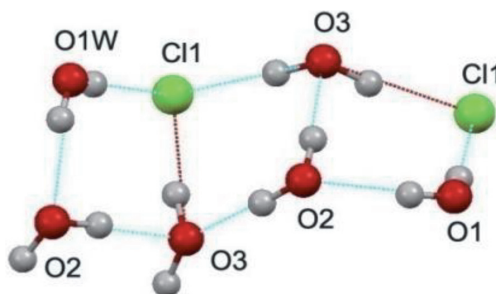


Figure 26.
Chair conformation formed by “water-chloride” cluster in complexes (6) and (7).

conformation. The three water molecules and a chloride molecule form a four-membered cyclic motif, and such three adjacent four-membered rings form the chair conformation (**Figure 26**).

4.3.5.1 Magnetic property and Mössbauer spectroscopy of complex (7)

The variable temperature (2.5–300 K) magnetic moment study shows the temperature dependence of the magnetic susceptibility. The χ_m values at 2.5 and 300 K are 0.33 and 0.005 cm³ mol^{−1}, while the μ_{eff} values are 2.61 and 3.46 B.M., respectively. The detailed study shows that the magnetic moment value consists of a superimposition of both the low-spin and high-spin states. At very low temperature, the 1-D supramolecular species which is formed by strong intermolecular C–H...O interactions and the cooperative interactions with the “water-chloride” cluster between mononuclear spin crossover (SCO) sites stabilize the low-spin state, and thus the high-spin contribution decreases to 21%, and the low-spin contribution increases to 79%. Thus, such variable temperature magnetic behavior may be due to a continuous $S = 1/2$ to $5/2$ spin crossover phenomenon of iron centers [36].

The Mössbauer spectroscopic study also supports that a spin crossover phenomenon exists in the iron(III) complex (7). Both the spin states, low ($S = 1/2$) and high ($S = 5/2$), exist in room temperature (300 K) as well as in very low temperature at 20 K. The population density of the electrons decreases from high-spin state to the low-spin state with decreasing temperature (**Table 1**).

| Temperature | Spin state | Occupancy |
|-------------|-----------------|-----------|
| 300 K | Low spin (1/2) | 49% |
| | High spin (5/2) | 51% |
| 20 K | Low spin (1/2) | 77% |
| | High spin (5/2) | 23% |

Table 1.
Population density at variable temperature in $[Fe(L^3)_2]Cl \cdot 3H_2O$ (7).

| Cell parameters | $[Zn(L^3)_2] \cdot 2H_2O$ (8) | $[Ni(L^3)(OAc)]$ (9) | $[Co(L^3)(OAc)] \cdot H_2O$ (10) | $[Cu(L^3)(OAc)] \cdot H_2O$ (11) |
|----------------------|-------------------------------|----------------------|----------------------------------|----------------------------------|
| System | Triclinic | Monoclinic | Monoclinic | Monoclinic |
| V (\AA^3) | 1294.88 | 810.3 | 1127.7 | 1044.17 |
| a (\AA) | 10.297368 | 6.364172 | 19.600876 | 18.953438 |
| b (\AA) | 11.32531 | 27.497931 | 5.53422 | 6.365518 |
| c (\AA) | 12.345947 | 4.686936 | 12.32786 | 8.729238 |
| α | 111.516869 | 90 | 90 | 90 |
| β | 103.288712 | 98.92 | 122.51 | 97.5 |
| γ | 91.155464 | 90 | 90 | 90 |

Table 2.
Powder X-ray diffraction data.

4.3.6 PXRD, SEM, and EDX studies of complexes (8)–(11)

Suitable single crystals of complexes (8)–(11) could not be grown even after repeated efforts; hence they were characterized by the powder X-ray diffraction study of the compounds [28, 29]. Some of the important lattice parameters of the PXRD study are summarized in **Table 2**.

The SEM investigation of all the above complexes, the ground powders, and the fracture surfaces indicates that the grain size distribution is not uniform, and submicron grains (finely ground powder) as well as grains (fracture surfaces) even above 20 μm (for complex 8) and above 10 μm (for complexes 9–11) have been observed [37, 38].

The formation of metal–ligand complexes and the presence of metal along with C and S within the metal complexes have been substantiated by the EDX analysis.

4.4 Electrical conductivity

To explore the utility of the metal complexes as functional materials, the electrical conductivity study was performed, and it shows the semiconducting nature of the complexes [33, 37, 38].

The samples for the measurement of electrical conductivity were prepared from the complexes in the form of tablets of approximately thickness ~ 0.1 cm at a pressure of ca. 1×10^8 Pascal. These tablets were placed between two copper electrodes covered with silver paste, and contacts of the prepared tablets were to be Ohmic or not. A two-probe method was used to investigate the electrical conductivities of the complex tablets by measuring the current through the probes with a high impedance electrometer (Keithley 6514) upon application of a DC voltage current supplied by a programmable source of voltage (Keithley 230). The conductivities were calculated by using the general equation of $\sigma = (I/V_c)(d/a)$, where (I) is

the current in ampere, V_c the potential drop across the sample of cross-sectional area (a), and is the thickness (d).

Variation of electrical conductivity of a compound behaving like semiconductor with temperature can be obtained by the Arrhenius equation:

$$\sigma = \sigma_0 \exp(-E_a/kT) \quad (1)$$

where σ is the electrical conductivity, σ_0 denotes the pre-exponential factor, E_a is the activation energy for this thermally activated process, and k is the Boltzmann constant. Generally, “log σ ” is plotted against “ $1000/T$ ” which is expected to have a linearly fitted graph. The thermal energy of activation (E_a) is determined from the slope of the graph.

If the graph obtained is linear (i.e., fitted with one straight line), then it may be concluded that no molecular rearrangement occurred during heating and the compound will have only one E_a . In this case the electrical conduction is mainly due to the intrinsic conducting property, whereas the nonlinear plot clearly indicates molecular rearrangement during heating of the compound. In case of nonlinear plot, more than one straight line are fitted against the linear parts of the plot. One straight line corresponding to lower temperature range is known as region I, and the other straight line corresponding to the higher temperature range is known as region II. In this case the compound will have two distinct energy of activations (E_{a1} and E_{a2}).

Conduction corresponding to the region I is attributed to the intermolecular conduction via weak force interactions between the molecules. The charge carriers hop near Fermi level within the localized state. Delocalized π -electrons are mainly responsible for this conduction, whereas conduction corresponding to the region II is attributed to intramolecular conduction between the metal center and the ligand center within a metal complex. This conduction occurs due to tunneling of electrons between equivalent HOMO and LUMO of the ligand and metal ion, respectively. Such tunneling of electrons through the intermolecular potential barrier is reinforced through π - π stacking and extensive H-bonding [24]. Depending on the availability of π -electrons, the compound behaves like n-type semiconductor.

From the Arrhenius plots (Figure 27), the electronic parameters, i.e., activation energy of electrical conduction (E_a) and the energy gap for directly allowed transitions of metal complexes (2) and (8–11), are calculated, and the results obtained are summarized in Table 3.

It is also very clear from the Arrhenius plots that the conductivity of metal complexes generally increases with increase in temperature. At room temperature

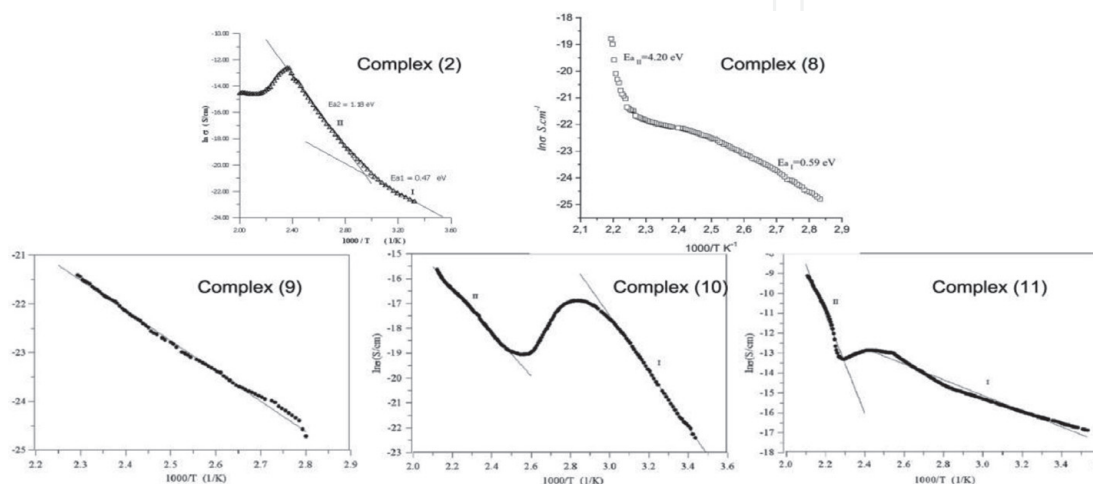


Figure 27.
 Temperature dependence. Electrical conductivity curves of the complexes [24, 28, 29].

| Complex | E _{a1} (eV) | E _{a2} (eV) | E _{gd} (eV) |
|---|----------------------|----------------------|----------------------|
| | (Lower temp) | (Higher temp) | |
| [VOL ²] (2) | 0.48 | 1.18 | 3.45 |
| [Zn(L ³) ₂].2H ₂ O (8) | 0.59 | 4.2 | 2.52 |
| [Ni(L ³)(OAc)] (9) | 0.54 | — | 2.75 |
| [Co(L ³)(OAc)].H ₂ O (10) | 0.97 | 0.76 | 2.37 |
| [Cu(L ³)(OAc)].H ₂ O (11) | 0.34 | 2.14 | 1.58 |

Table 3.
Activation energies and direct band gap values.

they behave as an insulator, while at higher temperature the semiconducting nature of complexes is observed.

4.5 Optical properties

Optical absorption spectra was taken by using a UV–VIS spectrophotometer (Perkin Elmer Lambda 2S/45 Double Beam) and measured as function of wavelength in the wavelength range 190–1100 nm.

The energy band gaps and the nature of the optical transitions involved in the metal complex framework systems have been practically determined by the fundamental absorption edge analysis of the recorded optical transitions using the theory of Mott and Davis [39]. It is also observed that the semiconducting behavior of a material increases with rise in temperature which may also damage the actual molecular structure of the material. Hence, Tauc method is used to calculate the energy band gap through optical absorption properties [40].

Utilizing the relation between the optical linear absorption coefficient (α) with photon energy ($h\nu$), the energy band gap (E_g) between the top of the valence band and bottom of the conduction band can be determined using equation (Eq. (2)):

$$\alpha h\nu = A(h\nu - E_g)^n \tag{2}$$

where A is a constant characteristic parameter of the respective transition independent of ν .

The values of n depend on the kind of optical transitions. For directly allowed, directly forbidden, indirectly allowed, and indirectly forbidden transitions, the values of n are 1/2, 3/2, 2, and 3, respectively. Thus the energy band gap for directly allowed (E_{gd}) and indirectly allowed (E_{gi}) transitions can be determined by relating Eq. (2) as follows:

$$\alpha h\nu = A_d(h\nu - E_{gd})^{1/2} \tag{3}$$

and

$$\alpha h\nu = A_i(h\nu - E_{gi})^2 \tag{4}$$

where E_{gd} and E_{gi} are direct and indirect energy gaps, respectively.

To calculate the direct and indirect energy band gap, we need to plot a curve of $(\alpha h\nu)^2$ against $f(h\nu)$ and $(\alpha h\nu)^{1/2}$ against $f(h\nu)$ and then by the extrapolation of the most linear part of the curve to zero.

The satisfactory graphs were obtained for the metal complexes (2) and (8)–(11) by plotting $(\alpha h\nu)^2$ against $f(h\nu)$. Therefore, the energy gaps determined correspond

to the direct energy gap (E_{gd}). The E_{gd} values of the metal complexes are collected in **Table 3**. The comparison of the band gap cannot be directly related to the atomic number of the metals in the complexes.

5. Conclusion

In this review, the synthesis, crystal structure, and solid-state properties of three Schiff base ligands derived from diacetylmonoxime with diethylenetriamine, 1,3-diaminopropane-2-ol, and morpholine N-thiohydrazide and their metal complexes have been vividly discussed. A zwitterionic nitrogen–sulfur heterocyclic compound with nonbonded S...S interaction has also been reported to be formed by the reaction of diacetylmonoxime with morpholine N-thiohydrazide under long refluxing (16 h) condition in ethanol. The single X-ray crystal structures have shown many beautiful weak force interactions including a $\text{CH}_3\cdots\text{O}$ trifurcated interface communication. Wherever the single-crystal structures could not be grown, the PXRD study has enlightened their structural features. The electrical and optical properties also explored the semiconducting nature of some of the metal complexes. It is also observed that the electron transport process gets influenced by the supramolecular frameworks of the metal complexes.

Acknowledgements

One of the authors (S.S.) is thankful to the UGC (ERO), Kolkata, for financial grants (MRP) to carry out a part of this work and also to Prof. Y. Aydogdu, Department of Physics, Gazi University, and Dr. S. Biswas, our lab-mate for some useful discussion.

Author details

Palash Mandal^{1,2}, Uttam Das³, Kamalendu Dey^{1†} and Saikat Sarkar^{4*}

1 Department of Chemistry, University of Kalyani, Kalyani, West Bengal, India

2 Lalgopal High (H.S.) School, Ranaghat, West Bengal, India


3 Department of Chemistry, Kalyani Government Engineering College, Kalyani, West Bengal, India

4 Department of Chemistry, Chakdaha College, Chakdaha, West Bengal, India

*Address all correspondence to: saikat_s@rediffmail.com

† Prof. Kamalendu Dey expired on September 01, 2019.

IntechOpen

© 2020 The Author(s). Licensee IntechOpen. This chapter is distributed under the terms of the Creative Commons Attribution License (<http://creativecommons.org/licenses/by/3.0>), which permits unrestricted use, distribution, and reproduction in any medium, provided the original work is properly cited. 

References

- [1] Yoon TP, Jacobsen EN. Privileged chiral catalysts. *Science*. 2003;**299**: 1691-1693. DOI: 10.1126/science.1083622
- [2] Slassi S, Aarjane M, Yamni K, Amine A. Synthesis, crystal structure, DFT calculations, Hirshfeld surfaces, and antibacterial activities of Schiff base based on imidazole. *Journal of Molecular Structure*. 2019;**1197**: 547-554. DOI: 10.1016/j.molstruc.2019.07.071
- [3] Qian HY, Sun N. Synthesis and crystal structures of manganese (III) complexes derived from bis-Schiff bases with antibacterial activity. *Transition Metal Chemistry*. 2019;**44**:501-506. DOI: 10.1007/s11243-018-00296-x
- [4] Sarkar S, Dey K. A series of transition and non-transition metal complexes from a N_4O_2 hexadentate Schiff base ligand: Synthesis, spectroscopic characterization and efficient antimicrobial activities. *Spectrochimica Acta Part A*. 2010;**77**:740-748. DOI: 10.1016/j.saa.2010.06.041
- [5] Sharma M, Chauhan K, Srivastava RK, Singh SV, Srivastava K, Saxena JK, et al. Design and synthesis of a new class of 4-aminoquinolinyl-and 9-anilinoacridinyl Schiff base hydrazones as potent antimalarial agents. *Chemical Biology & Drug Design*. 2014;**84**: 175-181. DOI: 10.1111/cbdd.12289
- [6] Ziegler J, Schuerle T, Pasierb L, Kelly C, Elamin A, Cole KA, et al. The propionate of heme binds N_4O_2 Schiff base antimalarial drug complexes. *Inorganic Chemistry*. 2000;**39**: 3731-3733. DOI: 10.1021/ic000295h
- [7] Chang EL, Simmers C, Knight DA. Cobalt complexes as antiviral and antibacterial agents. *Pharmaceuticals*. 2010;**3**:1711-1728. DOI: 10.3390/ph3061711
- [8] Chen Y, Li P, Su S, Chen M, He J, Liu L, et al. Synthesis and antibacterial and antiviral activities of myricetin derivatives containing a 1, 2, 4-triazole Schiff base. *RSC Advances*. 2019;**9**: 23045-23052. DOI: 10.1039/C9RA05139B
- [9] Venkateswarlu K, Ganji N, Daravath S, Kanneboina K, Rangan K. Crystal structure, DNA interactions, antioxidant and antitumor activity of thermally stable Cu (II), Ni (II) and Co (III) complexes of an N, O donor Schiff base ligand. *Polyhedron*. 2019;**171**:86-97. DOI: 10.1016/j.poly.2019.06.048
- [10] da Silveira VC, Luz JS, Oliveira CC, Graziani I, Ciriolo MR, da Costa Ferreira AM. Double-strand DNA cleavage induced by oxindole-Schiff base copper (II) complexes with potential antitumor activity. *Journal of Inorganic Biochemistry*. 2008;**102**: 1090-1103. DOI: 10.1016/j.jinorgbio.2007.12.033
- [11] Das U, Pattanayak P, Santra MK, Chattopadhyay S. Synthesis of new oxido-vanadium complexes: Catalytic properties and cytotoxicity. *Journal of Chemical Research*. 2018;**42**:57-62. DOI: 10.3184/174751918X15168821806597
- [12] Cozzi PG. Metal-Salen Schiff base complexes in catalysis: Practical aspects. *Chemical Society Reviews*. 2004;**33**: 410-421. DOI: 10.1039/B307853C
- [13] Gupta K, Sutar AK. Catalytic activities of Schiff base transition metal complexes. *Coordination Chemistry Reviews*. 2008;**252**:1420-1450. DOI: 10.1016/j.ccr.2007.09.005
- [14] Pouralimardan O, Chamayou AC, Janiak C, Hosseini-Monfared H. Hydrazone Schiff base-manganese (II) complexes: Synthesis, crystal structure and catalytic reactivity. *Inorganica*

Chimica Acta. 2007;**360**:1599-1608.
 DOI: 10.1016/j.ica.2006.08.056

252:1027-1050. DOI: 10.1016/j.ccr.2008.01.005

[15] Bagherzadeh M, Mahmoudi H, Ataie S, Hafezi-Kahnamouei M, Shahrokhian S, Bellachioma G, et al. Synthesis, characterization, and comparison of two new copper (II) complexes containing Schiff-base and diazo ligands as new catalysts in CuAAC reaction. *Inorganica Chimica Acta*. 2019;**492**:213-220. DOI: 10.1016/j.ica.2019.04.036

[16] Mondal P, Parua SP, Pattanayak P, Das U, Chattopadhyay S. Synthesis and structure of copper (II) complexes: Potential cyanide sensor and oxidase model. *Journal of Chemical Sciences*. 2016;**128**:803-813. DOI: 10.1007/s12039-016-1063-7

[17] Ghosh K, Banerjee A, Bauzá A, Frontera A, Chattopadhyay S. One pot synthesis of two cobalt (III) Schiff base complexes with chelating pyridyltetrazolate and exploration of their bio-relevant catalytic activities. *RSC Advances*. 2018;**8**:28216-28237. DOI: 10.1039/C8RA03035A

[18] Sedighipoor M, Kianfar AH, Mohammadnezhad G, Görls H, Plass W. Unsymmetrical palladium (II) N, N, O, O-Schiff base complexes: Efficient catalysts for Suzuki coupling reactions. *Inorganica Chimica Acta*. 2018;**476**:20-26. DOI: 10.1016/j.ica.2018.02.007

[19] Andruh M, Branzea DG, Gheorghe R, Madalan AM. Crystal engineering of hybrid inorganic-organic systems based upon complexes with dissymmetric compartmental ligands. *CrystEngComm*. 2009;**11**:2571-2584. DOI: 10.1039/B909476H

[20] Ganguly R, Sreenivasulu B, Vittal JJ. Amino acid-containing reduced Schiff bases as the building blocks for metallasupramolecular structures. *Coordination Chemistry Reviews*. 2008;

[21] Liu X, Hamon JR. Recent developments in penta-, hexa-and heptadentate Schiff base ligands and their metal complexes. *Coordination Chemistry Reviews*. 2019;**389**:94-118. DOI: 10.1016/j.ccr.2019.03.010

[22] Furukawa H, Cordova KE, O'Keeffe M, Yaghi OM. The chemistry and applications of metal-organic frameworks. *Science*. 2013;**341**:1230444(1-12). DOI: 10.1126/science.1230444

[23] Li C, Tang H, Fang Y, Xiao Z, Wang K, Wu X, et al. Bottom-up assembly of a highly efficient metal-organic framework for cooperative catalysis. *Inorganic Chemistry*. 2018;**57**:13912-13919. DOI: 10.1021/acs.inorgchem.8b02434

[24] Xiong G, Chen XL, You LX, Ren BY, Ding F, Dragutan I, et al. La-metal-organic framework incorporating Fe₃O₄ nanoparticles, post-synthetically modified with Schiff base and Pd. A highly active, magnetically recoverable, recyclable catalyst for CC cross-couplings at low Pd loadings. *Journal of Catalysis*. 2018;**361**:116-125. DOI: 10.1016/j.jcat.2018.02.026

[25] Ross TM, Neville SM, Innes DS, Turner DR, Moubaraki B, Murray KS. Spin crossover in iron (III) Schiff-base 1-D chain complexes. *Dalton Transactions*. 2010;**39**:149-159. DOI: 10.1039/B913234A

[26] Yang H, Liu SS, Meng YS, Zhang YQ, Pu L, Yu XQ. Magnetic properties and theoretical calculations of mononuclear lanthanide complexes with a Schiff base coordinated to Ln (III) ion in a monodentate coordination mode. *Inorganica Chimica Acta*. 2019;**494**:8-12. DOI: 10.1016/j.ica.2019.04.051

- [27] Miyasaka H, Clérac R, Wernsdorfer W, Lecren L, Bonhomme C, Sugiura KI, et al. A dimeric manganese (III) tetradentate Schiff base complex as a single-molecule magnet. *Angewandte Chemie International Edition*. 2004;**43**: 2801-2805. DOI: 10.1002/anie.200353563
- [28] Nandy M, Shit S, Rosair G, Gómez-García C. Synthesis, characterization and magnetic studies of a tetranuclear manganese (II/IV) compound incorporating an amino-alcohol derived Schiff base. *Magnetochemistry*. 2018;**4**: 57-67. DOI: 10.3390/magnetochemistry4040057
- [29] Sarkar S, Nag SK, Chattopadhyay AP, Dey K, Islam SM, Sarkar A, et al. Synthesis, structure and catalytic activities of nickel (II) complexes bearing N₄ tetradentate Schiff base ligand. *Journal of Molecular Structure*. 2018;**1160**:9-19. DOI: 10.1016/j.molstruc.2018.01.035
- [30] Sarkar S, Biswas S, Liao MS, Kar T, Aydogdu Y, Dagdelen F, et al. An attempt towards coordination supramolecularity from Mn (II), Ni (II) and Cd (II) with a new hexadentate [N₄O₂] symmetrical Schiff base ligand: Syntheses, crystal structures, electrical conductivity and optical properties. *Polyhedron*. 2008;**27**:3359-3370. DOI: 10.1016/j.poly.2008.07.034
- [31] Costes JP, Duhayon C, Vendier L, Mota AJ. Reactions of a series of ZnL, CuL and NiL Schiff base and non-Schiff base complexes with MCl₂ salts (M = Cu, Ni, Mn): Syntheses, structures, magnetic properties and DFT calculations. *New Journal of Chemistry*. 2018;**42**:3683-3691. DOI: 10.1039/C7NJ04347C
- [32] Majumdar D, Das D, Sreejith SS, Das S, Biswas JK, Mondal M, et al. Dicyanamide-interlaced assembly of Zn (II)-Schiff-base complexes derived from salicylaldimino type compartmental ligands: Syntheses, crystal structures, FMO, ESP, TD-DFT, fluorescence lifetime, in vitro antibacterial and anti-biofilm properties. *Inorganica Chimica Acta*. 2019;**489**:244-254. DOI: 10.1016/j.ica.2019.02.022
- [33] Sarkar S, Aydogdu Y, Dagdelen F, Bhaumik BB, Dey K. X-ray diffraction studies, thermal, electrical and optical properties of oxovanadium (IV) complexes with quadridentate Schiff bases. *Materials Chemistry and Physics*. 2004;**88**:357-363. DOI: 10.1016/j.matchemphys.2004.08.001
- [34] Biswas S, Yap GP, Dey K. Reaction of diacetylmonoxime with morpholine N-thiohydrazide in the absence and in presence of a metal ion: Facile synthesis of a thiadiazole derivative with non-bonded S...S interaction. *Polyhedron*. 2009;**28**:3094-3100. DOI: 10.1016/j.poly.2009.06.091
- [35] Biswas S, Sarkar S, Steele IM, Sarkar S, Mostafa G, Bhaumik BB, et al. Two-dimensional supramolecular assembly of phenylmercury (II) and cadmium (II) complexes with a tridentate thiohydrazone NNS donor ligand: Synthesis, coordination behavior and crystal structure. *Polyhedron*. 2007;**26**:5061-5068. DOI: 10.1016/j.poly.2007.07.027
- [36] Saha R, Biswas S, Steele IM, Dey K, Mostafa G. A supramolecular spin crossover Fe (III) complex and its Cr (III) isomer: Stabilization of water-chloride cluster within supramolecular host. *Dalton Transactions*. 2011;**40**: 3166-3175. DOI: 10.1039/C0DT01256D
- [37] Dagdelen F, Aydogdu Y, Dey K, Biswas S. Synthesis, characterization and solid-state properties of [Zn (Hdmmthiol)₂].2H₂O complex. *The European Physical Journal Plus*. 2016;**131**:143-150. DOI: 10.1140/epjp/i2016-16143-2

[38] Biswas S, Dagdelen F, Aydogdu Y, Dey K. Structural, electrical and optical properties of metal complexes of NNS donor ligand. *Materials Chemistry and Physics*. 2011;**129**:1121-1125. DOI: 10.1016/j.matchemphys.2011.05.071

[39] Mott NF, Davis EA. *Electronic Processes in Non-crystalline Materials*. Oxford: Clarendon Press; 1971. DOI: 10.1002/crat.19720070420

[40] Tauc J, Grigorovici R, Vancu A. Optical properties and electronic structure of amorphous germanium. *Physica Status Solidi B*. 1966;**15**:627-637. DOI: 10.1002/pssb.19660150224